The Response of Metal Nanoparticles in Comparison with That of Apertures with FDTD Simulation and the Application of Single Channel Limit

by

Wen Ma

B.Eng, Dalian University of Technology, 2012

A Project Report Submitted in Partial Fulfillment

of the Requirements for the Degree of

Master of Engineering

in the Electrical and Computer Engineering Department

Supervisory Committee

The Response of Metal Nanoparticles in Comparison with That of Apertures with FDTD Simulation and the Application of Single Channel Limit

by

Wen Ma
B.Eng, Dalian University of Technology, 2012

Supervisory Committee

Reuven Gordon, Electrical and Computer Engineering Department
Supervisor

Poman P. M. So, Electrical and Computer Engineering Department
Co-Supervisor or Departmental Member

Abstract

Supervisory Committee

Reuven Gordon, Electrical and Computer Engineering Department
Supervisor

Poman P. M. So, Electrical and Computer Engineering Department
Co-Supervisor or Departmental Member

Finite-Difference Time-Domain (FDTD) method is playing an important role in solving the Maxwell equation because the FDTD algorithm is a relatively fast method. While the simplicity is definitely another reason why the FDTD was used widely, the FDTD is also able to solve extremely complicated engineering problems.

For the situation of typical electric dipole transition, the maximum scattering cross section of the subwavelength nanoparticle can be proved to be $3\lambda^2/2\pi$. This limit from standard scattering theory was named the single channel limit.

In this report, we will apply FDTD method to implement several simulations and investigate the relationship between the response and the single channel limit.

Table of Contents

List of Figures

Abbreviations:

FDTD	Finite Difference Time Domain
DGTD	Discontinuous Galerkin Time Domain
ABC	Absorbing Boundary Condition
PML	Perfectly Matched Layer
PEC	Perfect Electric Conductor
SP	Surface Plasmon
SRR	Split-Ring Resonator
TFSF	Total Field Scattered Field

Maxwell's Equation involved in this report

1. $\nabla \cdot \mathbf{D} = \rho_v$
2. $\nabla \cdot \mathbf{B} = 0$
3. $\nabla \times \mathbf{E} = -\frac{\partial \mathbf{B}}{\partial t}$
4. $\nabla \times \mathbf{H} = \frac{\partial \mathbf{D}}{\partial t} + \mathbf{J}$

Chapter 1 Introduction

1.1 General Introduction

Finite-Difference Time-Domain (FDTD) method is playing an important role in solving the Maxwell equation because the FDTD algorithm is a relatively fast method. While the simplicity is definitely another reason why the FDTD was used widely, the FDTD is also able to solve extremely complicated engineering problems.

The motivations of this work come from that we try to investigate the similarity between apertures and nanoparticles and the FDTD method is such a proporate tool to implement that.

First, with FDTD method, we will prove that apertures and nanoparticles behave in a very similar fashion and compare their maximum E fields. Second, we will investigate when the aperture gets the maximum absorption. Third, we will simulate the transition from a straight dipole nanoparticle to a split-ring resonator with FDTD method. Previous work was based on the discontinuous Galerkin time-domain (DGTD) method. Fourth, we will demonstrate that in a single aperture system, the forward scattering is equal to the backward scattering. Lastly, we will determine the transmission for a single aperture system with a thickness of 100nm. In each of the above cases, the extinction, scattering and absorption will be compared with the single channel limit.

1.2 Report Outline

This report is organized into 5 chapters. Chapter 2 provides the theoretical basis for the

FDTD method and the Single Channel Limit, as well as reviews on some of the pioneering works of FDTD method. Chapter 3 introduces the whole process of the simulation. Chapter 4 shows the derivation of the theory of the Single Channel Limit. Lastly, conclusions and summary are provided in Chapter 5.

Chapter 2 Background

2.1 FDTD Method

Kane S.Yee first proposed the Finite-Difference Time-Domain method in 1966 [1]. A discrete solution to Maxwell's equations was proposed which was based on central difference approximations of derivatives of the curl-equations. The approach contributed to the staggering of the electric and magnetic fields in both space and time so that it could obtain second-order accuracy. A three-dimensional formulation was derived, and the method was validated by Yee with two-dimensional problems. Yee's method was not widely accepted until 1975 when Taflove and Brodwin used Yee's method to make a simulation for the scattering by dielectric cylinders [2] and biological heating [3]. In 1977, this method was applied by Holland to determine the currents induced on an aircraft [4].

The increasing use of the FDTD method since the 1970's can be associated with the significant advances in computer technology. Nowadays, a grid dimension of 4,000 $\times$4,000 $\times$4,000 is accessible due to the technology of parallel computers. Besides that, the speed of the FDTD algorithm outruns most of its counterparts. If K is the total number of degrees of freedom in a 3D space, every time-iteration merely requires O(K) floating-point operations. The discrete mesh should fill the full three-dimensional space. The number of degrees of freedom changes cubically with the linear dimension of the corresponding domain. The simplicity is definitely a reason why the FDTD was used widely. Even though the FDTD method is a simple method that can be taught at the undergraduate and early graduate stage, the FDTD is able to solve extremely

sophisticated engineering problems.

To simulate some unbounded problems, the discrete domain must be reduced through an absorbing boundary without any reflection.A second-order accurate absorbing boundary condition (ABC) was developed by Mur in 1981 [5] which contributed to solving this problem. Afterwards, more versatile boundary operators were introduced by Higdon [6]. Higdon's absorbing boundary condition was extended by Betz-and Mittra to absorb evanescent waves [7]. As these absorbing boundary conditions were authoritatively used, the range of the FDTD method and applications was then limited by the absorbing boundaries. By the Perfectly Matched Layer (PML) absorbing medium, J.-P. Berenger put forward a more accurate absorbing boundary [8]. The perfectly matched layer can provide smaller reflection error than that provided by an absorbing boundary condition. The PML can also be used to truncate unbounded media. Berenger's PML was developed further to absorb evanescent waves and near fields. The disadvantages of the PML are the increase of the mesh region and extra degrees of freedom in the PML region. It calls for more computational resourses than a local ABC. In the 1990's, these resources became reachable even with commodity computers, as a result, the FDTD method with PML absorbing boundaries was able to be applied to a broader range of situations.

One of the good points of the FDTD method is that any media types can be simulated. Inhomogeneous and lossy media was accommodated by the FDTD method naturally. FDTD method involves more complex media types like anisotropic, bi-anisotropic, chiral, and non-linear media. The researchers have made much effort to

develop accurate and efficient method to model such media.. F. L.Teixeira made an excellent summary of how to handle complicated media [9].

Since the fundamental Yee-method is limited to a regularly-spaced orthogonal grid, it fails to be revisable for some high-fidelity simulation of complex geometries. One way the method has been improved is through the use of the techniques modeling subcells. Subcell models make use of local approximations to resolve the fields near geometric features accurately. Simpson and Holland proposed the first subcell model as early as 1981 for the simulation of thin wires set in the FDTD grid [10]. Many subcell models were proposed for different kinds of applications since then. A kind of subcell model succeed in enhancing the precision of the local fields without reducing stability of the algorithm and evidently cutting down the time-step. Another method which can resolve fine geometric features is that we introduce local sub-grids. In that case, a sub-grid is embedded into the global grid so that fine geometric structure can be resolved locally without reducing the global space.It is very important to introduce subcell models and sub-gridding methods in improving the efficiency and the precision of the FDTD method in the case of very complex systems.

As the usage of the FDTD method grows, the application field it has influenced has shown diversity. The FDTD method was applied mainly to classical field in electromagnetics initially, including wave propagation, electromagnetic compatibility, microwave circuits, antennas and electromagnetic scattering. Nowadays, the FDTD method has also been applied to many other fields, including biomedical engineering, electromagnetic environmental hazards, ground penetrating radar, photonics,

biophotonics, plasmonics, photovoltaics, nano-optical storage devices, and seismic detection [11].

The FDTD method is developing very quickly. More general gridding techniques, unconditionally stable schemes,and multiphysics applications contribute to the development of the current FDTD method.With these effort and growing advances in computing technology, the FDTD method will definitely continue to be improved.

Limitation of the FDTD method [12]

When considering the history of the FDTD method, the former section presents different kinds of benefits of the FDTD method. Of course, the method definitely has its flaw, and there is a need to point out what these are.It is necessary to learn about the limitations of the FDTD method so that we can decide when the method is suitable. One of the disadvantages of the FDTD method is that it calls for a full discretization of the electric and magnetic fields through the whole domain. There are lots of examples while the FDTD method is used to simulate some “white-space”. The electromagnetic scattering of perfectly conducting spheres could be one of the instances. The region inside each sphere would be part of the white space.The region between the spheres and the region separating the spheres from the absorbing boundary would be the other part. The separation between the spheres is related to the percentage of white space. The feature that the FDTD method is completely explicit could also be viewed as a defect, while it is counted as a strength with a premise of that a linear system of equations is not required to be resolved, which may be a weakness since the time-step becomes

inordinately small. The smallest geometric feature in the model limits the time-step .Based on that, models with electrically small geometric features could fulfill very small time-steps, which can result in many time-iterations. It will be challenging when we apply the FDTD method to large scale of problems with fine geometric features that have to be modeled.

A broad frequency response can be studied by a single simulation on a count of that the broad-band simulation was provided by the FDTD method. Again, in many situations, this can be counted as an advantage, nevertheless there are some examples that only a narrow band response is acceptable. Consequently, a frequency domain simulation would be much more efficient. In addition, when modeling materials with complex constants, if the constants are only given over a narrow frequency band, the material have to be modeled over a broadband by the FDTD method. This could be as easy as the loss tangent of a substrate, or the effective material properties of a metamaterial. The FDTD method could be challenged when the system under modeling has a very high Q. As a result, the time-domain simulation could take a very long time to attain a steady state, because of narrow band resonances which decay slowly. It results in a long simulation time.In some situations, this can be reduced by using the methods such as the Generalized Pencil of Functions [13] to determine the resonances, or to infer the signal. In other situations, a frequency-domain simulation can be easier to use. The orthogonal gridding also restrains the FDTD method, which can be improved by the development of subcell modeling techniques and sub-gridding and non-uniform grid methods. However, the accuracy is still low in local fields. With the

method of subcell modeling, there is a worry of uncertainty as to the detailed shape of the local boundary. Thus, it is necessary to study the accuracy of the near fields which can be attained by subcell models. Higher-order FDTD methods did not copy the success of higher-order algorithms listed even if it used discontinuous Galerkin methods [14,15]. Many higher-order FDTD methods refer to an extended stencil, in other words, they indicate high-order difference approximations that take points that cover several grid cells, which makes it difficult to model easy geometries that include the jump discontinuities in the materials. The structures with fine geometric detail also challenge these methods.

2.2 Single Channel Limit

While the subwavelength nanoparticle is a single object in a three dimensional (3D) free space,it can be proved that its maximum scattering cross section is $(2l+1)\lambda^2/2\pi$ at the atomic resonant frequency, where l is the total angular momentum of the atomic transition involved[16]. This limit changes to $3\lambda^2/2\pi$ for the situation of typical electric dipole transition [17]. Similarly, in two dimensions, it can be proved that the maximum cross section of an atom cannot go over $2\lambda/\pi$. These limits in 3D or 2D, from standard scattering theory were named as the single channel limit.

Most of the nanostructures do have their maximum cross section according to the single-channel limit, and besides that, in plasmonic nanoparticles or nanowires, there is in fact a chance to evidently overcome this limit. As a numerical derivation, a subwavelength plasmonic structure was proposed where the scattering cross section is

far beyond the single channel limit, even in term of loss.

For subwavelength objects, those angular momentum not supporting a resonance usually contribute little to the total scattering cross section.Thus, if resonance is existing in only one angular momentum channel, the total scattering cross section is limited by the single-channel limit ($2\lambda/\pi$ in 2D, and $(2l+1)\lambda^2/2\pi$ in 3D). Such a single channel limit can be overcame, by setting resonances in many channels.

It is necessary to study basic limits on the emitted light intensity. It is implied by Kirchhoff's law that the emittance of an object is always less than that of an ideal black-body. The radiative features of planar black-body structures are well studied and the application of Kirchhoff's law is easy to understand.

With Mie theory, basic limits on the extinction, scattering and absorption of nano structures are derived .The condition derived for maximal absorption is the same with that of maximum power transfer in the antenna theory. The maximal potential absorption cross-section is given by $Q_{abs,m} = 1/2ka$ ($Q_{abs,m} = \lambda/2\pi$), where k is the vacuum wave vector and a is the radius of the particle.

Chapter 3 Simulation

3.1 Simulation of 100nm Silver Film

3.1.1 Introduction

Based on the previous work[18], Fig 3.1a and Fig 3.1b describe the normalized-to-area transmission spectra for the three group of parameters. For the case of a rectangular hole located on a perfect conductor, a transmission resonance exists at the corresponding cutoff wavelength [19]. The cutoff condition, which limits the maximum wavelength of light propagating in a waveguide, is decided by the wavelength where the propagation constant of the lowest order waveguide mode is zero. For a rectangular hole drilled on a metal, a transmission resonance existed at the cutoff wavelength. Fig 3.1b describes the redshift in the transmission crest wavelength with reducing short-edge width of the hole and that transmisssion is increasing with the ratio a_x and a_y. The simulation above is based on the 300nm thickness, and in our following simulation, we want to discover if the conclusion remains the same when we change the thickness to 100nm.

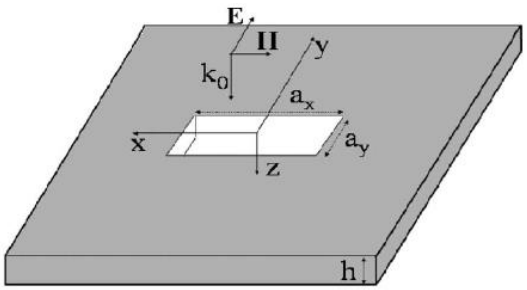

Fig 3.1a the diagram of a single rectangular hole (with long edge a_x and short edge a_y) drilled on a silver film of thickness h. The structure is described by a normally p-

polarized incident wave with its E-field vector perpendicular to the x axis.

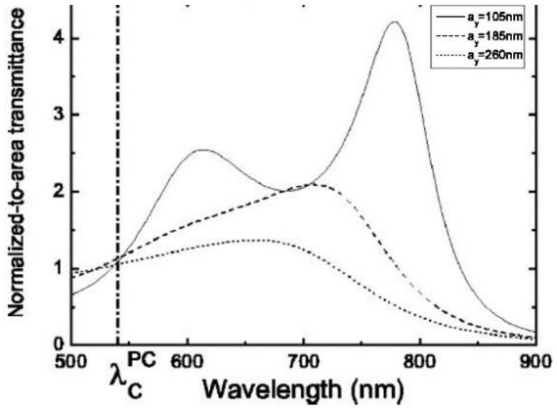

Fig 3.1b Normalized-to-area transmittance for rectangular holes with a_x=270 nm and a_y=105, 185, and 260 nm drilled on a silver film with h=300 nm.

3.1.2 Simulation Details

Perfectly matched layer boundary conditions were employed against reflection of the outgoing waves. The meshing area within the perfectly match layer was 300nm by 300nm . The grid sizes along the x and y directions were 5 nm, and along the z direction it was 3 nm, which contribute to better resolution along the direction of propagation of the wave.

A normally incident excitation wave was employed, a broadband pulse of 3.3 fs polarized along the short edge of the hole. The simulation was fulfilled for a 200 fs integration time. A frequency domain power monitor was set on the exit side to capture the transmission. The thickness of the film was fixed at 100nm and the corresponding transmissions at the exit side were recorded.

The result shows below,

(Dimensions: long edge:270nm; short edge:105nm,185nm,260nm;height:100nm)

(Material:Ag(silver)-Palik(0-2um))

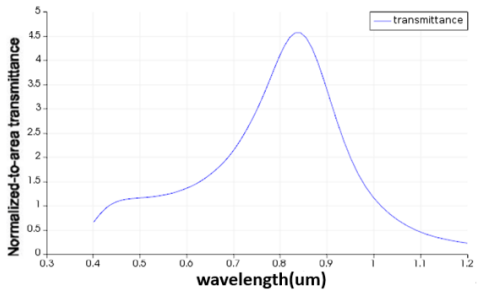

Fig 3.2 the transmittance of the structure with 105nm short edge

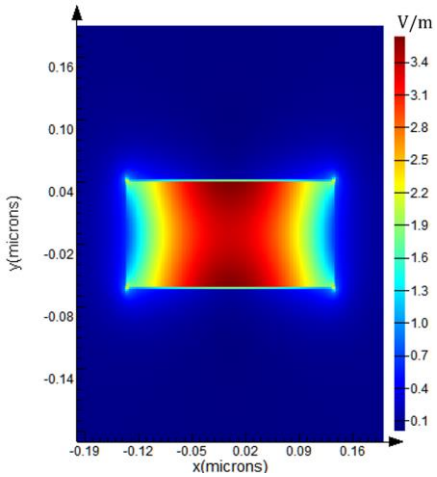

Fig 3.3 E field profile at the x-y plane for 105nm short edge

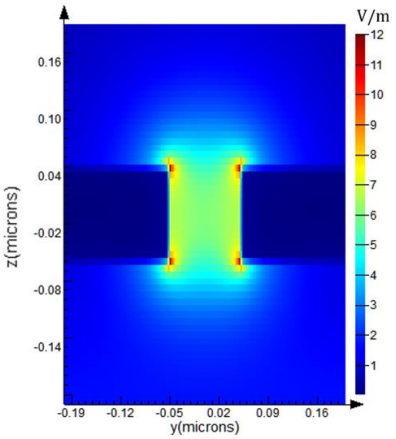

Fig 3.4 E field profile at the y-z plane for 105nm short edge

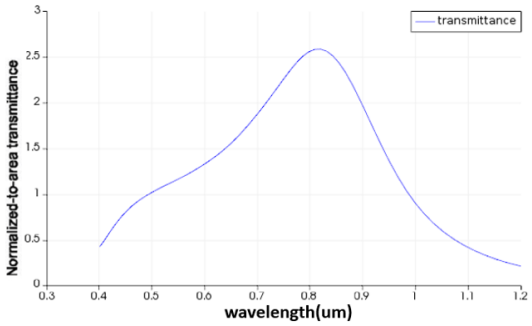

Fig 3.5 the transmittance of the structure with 185nm short edge

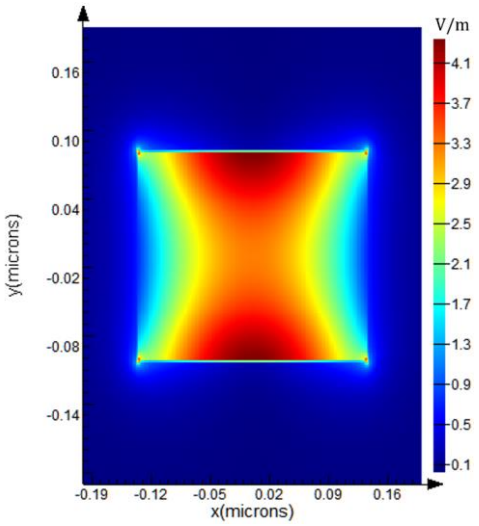

Fig 3.6 E field profile at the x-y plane for 185nm short edge

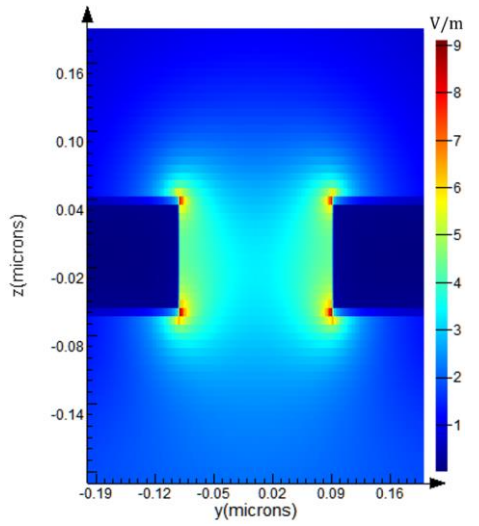

Fig 3.7 E field profile at the y-z plane for 185nm short edge

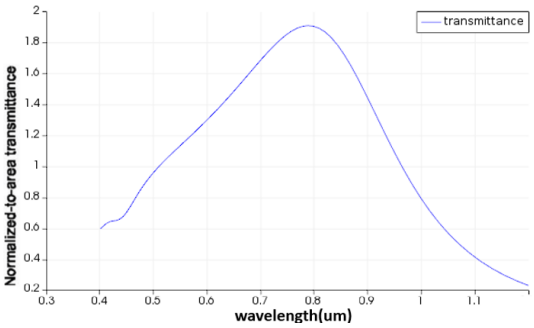

Fig 3.8 the transmittance of the structure with 260nm short edge

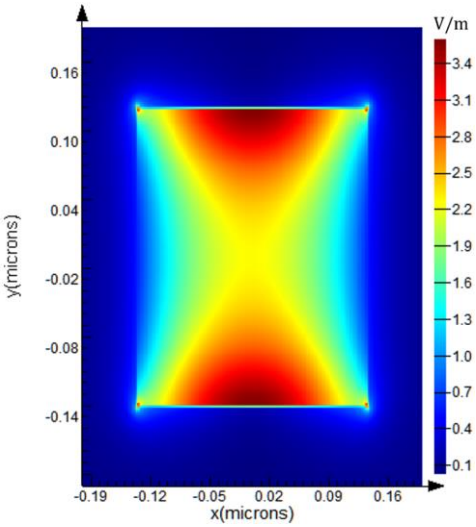

Fig 3.9 E field profile at the x-y plane for 260nm short edge

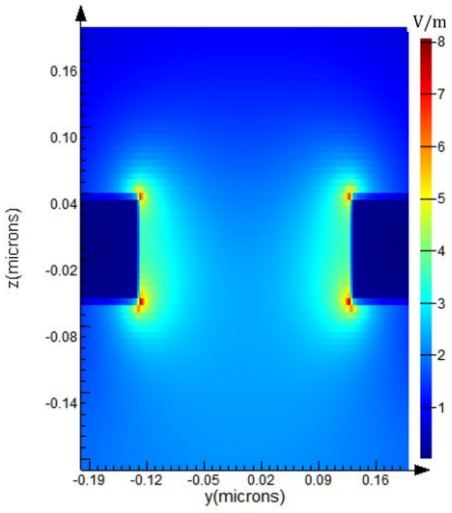

Fig 3.10 E field profile at the y-z plane for 260nm short edge

3.1.2 Summary and Discussion

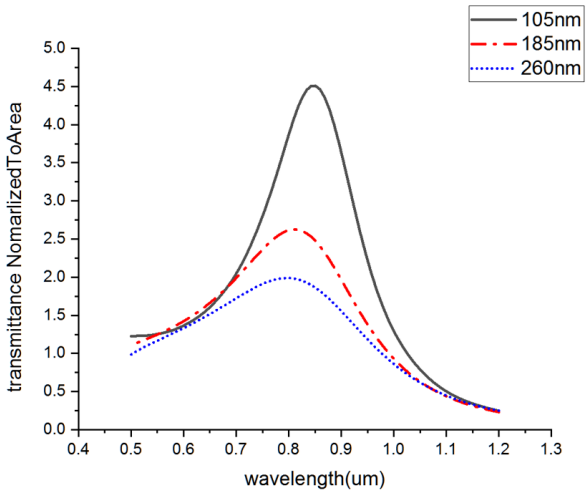

Fig 3.11 overview of the response of the 100nm silver film

With 100nm silver film we can also see the redshift in the transmission peak wavelength with cutting down width of the hole and that transmittance is increasing with the ratio length of long edge over length of short edge.

The cutoff condition for a rectangular hole, for which no light can propagate through the hole in a perfect electric conductor (PEC), happens when the wavelength of light is more than twice the hole-length across[20].

When rectangular holes were periodically distributed,the transmission is decided by the aspect ratio of the hole [21]. The maximum transmission through the hole was red-shifted when the hole was smaller, because of the effect of the Surface Plasmon(SP) coupling between the edges of the aperture [22,23]. In our simulation, we can clearly see the red-shift in the transmission peak wavelength with cutting down width of the hole, which is in agreement with the results above.

we consider the analytic theory of light transmission through a rectangular aperture

in a real metal and use this theory to show the significant increase in the cutoff wavelength when the hole size was made smaller. The finite- difference calculations confirmed the results. And the transmission resonance was simulated by finite-difference time-domain (FDTD) method and numerical mode analysis. The amplitude of the reflection from the impedance difference between the hole and the vacuum are extracted from the FDTD calculations.

3.2 Backward Scattering and Forward Scattering

3.2.1 Introduction

In this part, we use FDTD method to prove that the forward scattering of the aperture is equal to its backward scattering.And both of them are under single channel limit.

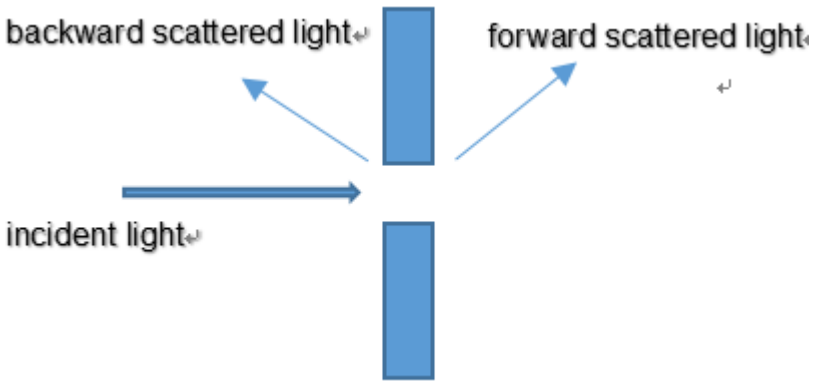

Fig 3.12 when the incident light reaches the structure, backward scattered light and forward scattered light can be observed

3.2.2 Simulation Details

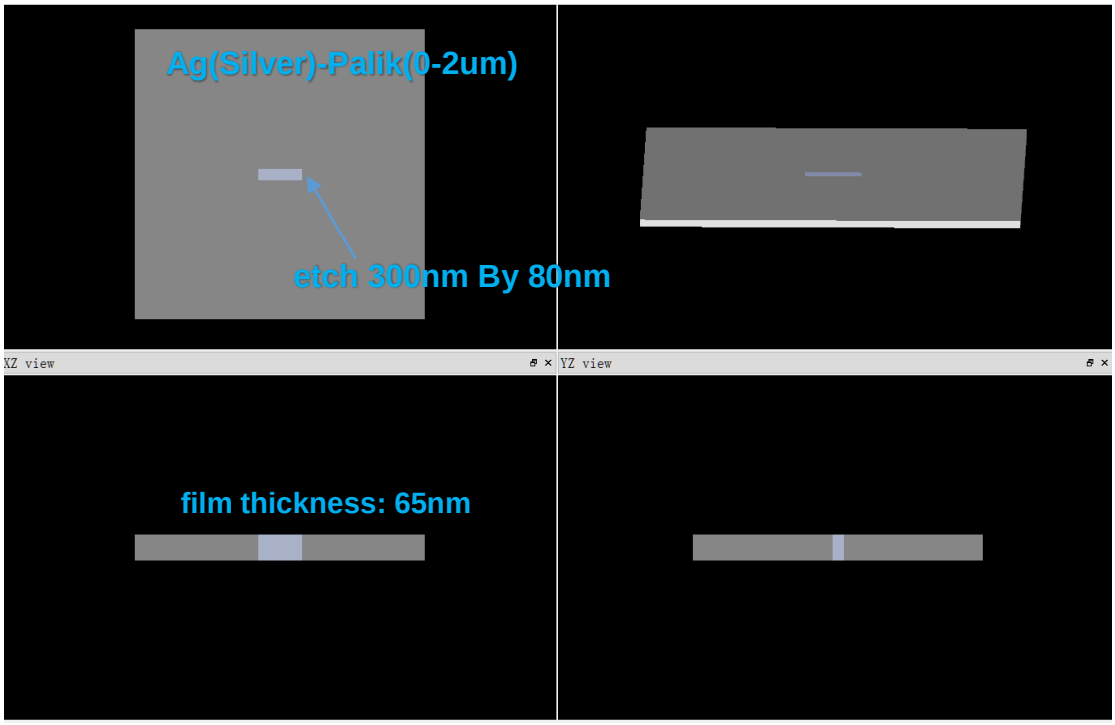

Fig 3.13 the dimensions of the structure

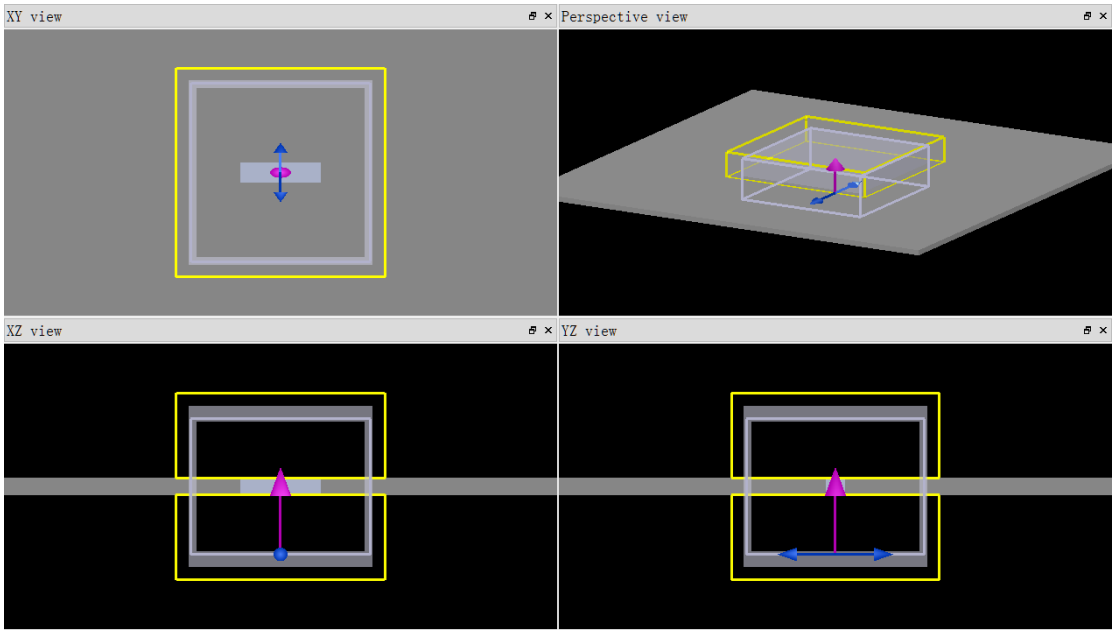

Fig 3.14 The simulation region within the perfectly match layer was 400nm by 400 nm . The grid accuracy along the x and y directions were 5 nm, while along the z direction it was 3 nm, which contributed better resolution along the direction of propagation of the wave.

A normal Total-Field Scattered-Field was used to exclude the influence of the metal reflection, a broadband pulse of 3.3 fs polarized perpendicular to the long edge of the

hole. The simulation was performed for an integration time of 200 fs. Two analysis group of power monitors were placed on the exit side and the entrance side individually to calculate the cross section of the scattered light. (The scripts of the monitor were changed to make only five sides in each group of monitors calculated and the calculation for the side next to silver film was removed.)

3.2.3 Results and Discussion

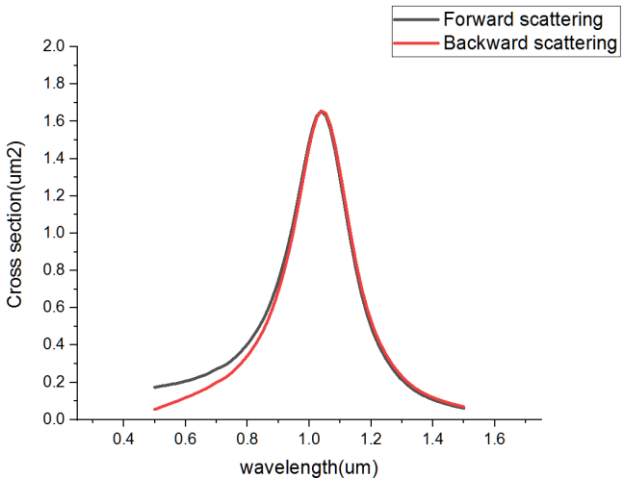

Fig 3.15 the response of a silver film with a rectangular aperture in it

By the simulation, It is proved that the backward scattering is almost the same with the forward scattering.

3.3 Transition from a Straight Dipole antenna to a Split Ring Resonator.

3.3.1 Introduction

Based on the previous work, the changes from a gold dipole nano-structure in a line to a split-ring resonator was studied [24,25]. In fact, this means that a straight metal wire with fixed length was bent into a closed ring. As we all know, this transition did not change the resonance wavelength much, providing a direct comparison. The previous simulation was implemented with the traditional discontinuous Galerkin time-domain (DGTD) method. And now I use FDTD method to simulate that.

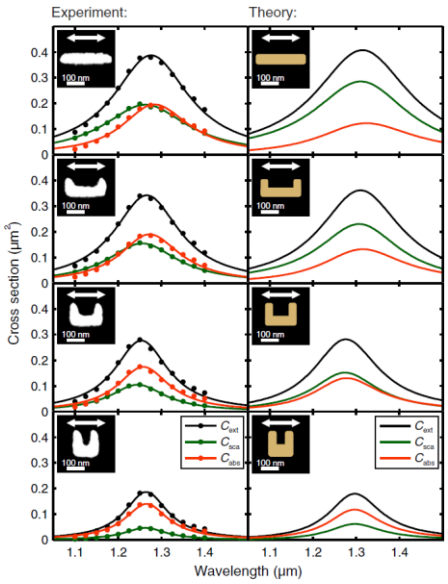

Fig 3.16 This group of figures describes the changes from a straight dipole antenna (top) to a split-ring resonator (bottom). In the left part, the figures show the determined absorption cross-section, scattering cross-section , and extinction cross-section profile. The solid lines come from Lorentzian fits. The figures describe the response of the 35 nm thin Au nano structures. The incident wave is perpendicular to the short edge (y axis). The results of corresponding numerical calculations are shown in the right part with the same scale and format to compare directly with the left part. In each figure, the dismatch between extinction and scattering cross-section shows the absorption cross-section.

3.3.2 Simulation Details

simulation parameter	
Material	Au
Au film thickness	35nm
SiN film thickness	30nm
Si substrate thickness	200nm

Table 3.1 the parameter for the simulation.

The reflection of the outgoing waves was prevented by the perfectly match layer (PML) boundary conditions. The simulation region within the perfectly match layer was 600nm x 600 nm. The grid accuracy along the x and y directions were 2 nm, while along the z direction it was 6 nm, which was done to have more accurate resolution along the direction of x axis and y axis.

A normally incident excitation field was used, a broadband pulse of 3.3 fs polarized perpendicular to the long edge of the hole. The simulation was carried out for an integration time of 200 fs.

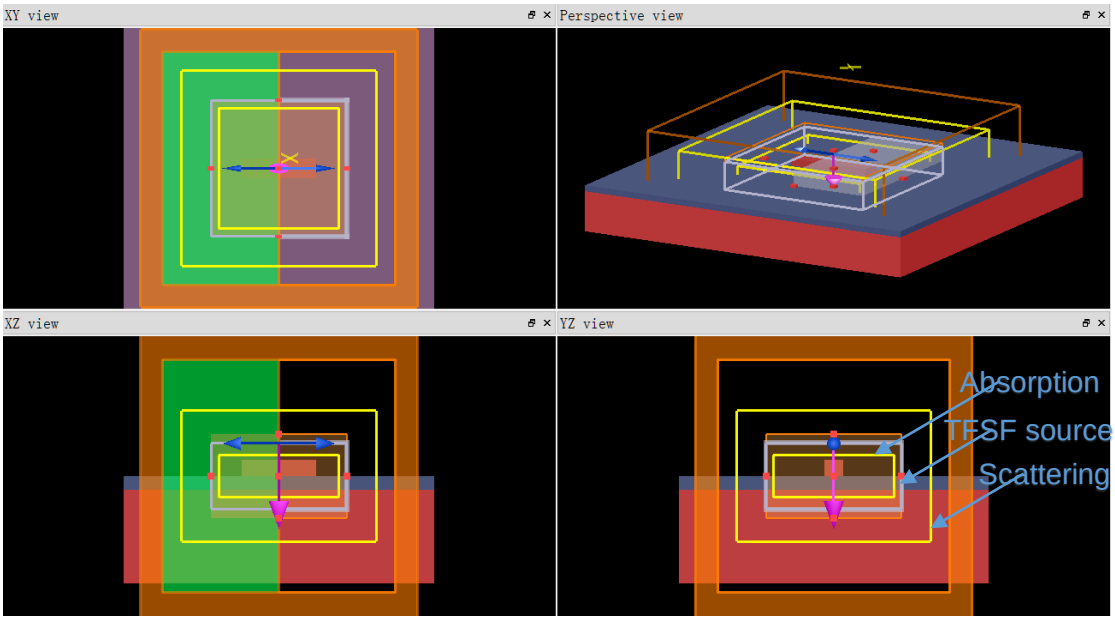

Fig 3.17 Background index was set to be 1,the simulation time was 200fs, and simulation temperation was 300K. Besides that, x min boundary condition was set to be Anti-Symmetric,and source wavelength ranged from 1000nm to 1500nm.

3.3.3 Results and Discussion

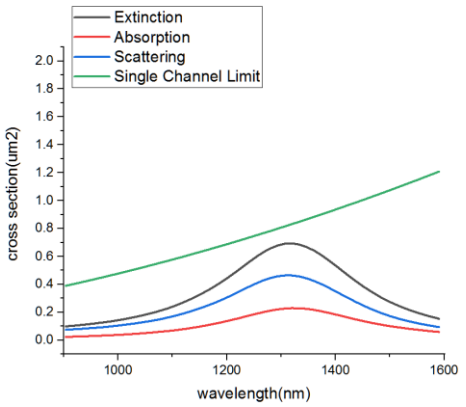

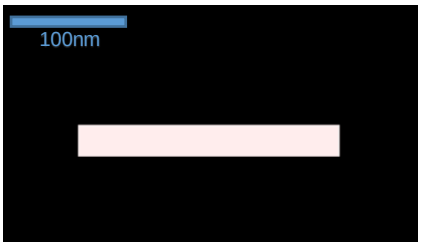

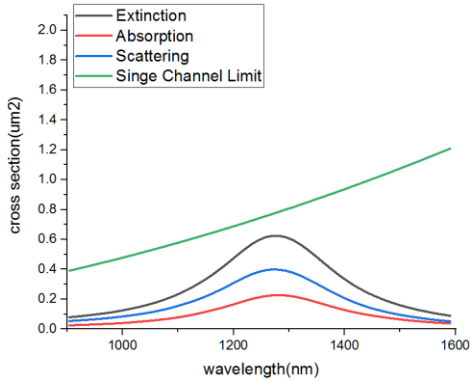

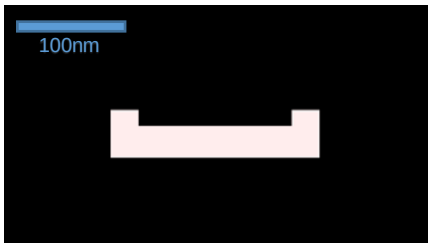

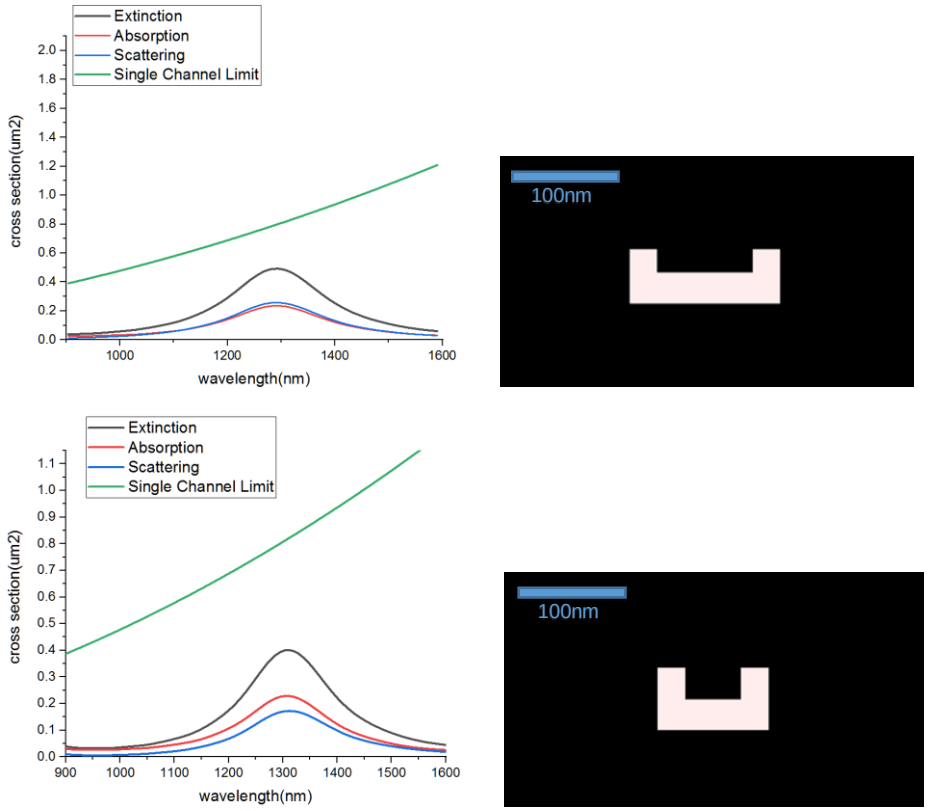

Fig 3.18 as changing the shape of the structure like the figures right-hand side above, the scattering is increasing while the absorption is decreasing and eventually the absorption exceeds the scattering. With the FDTD method, we can see the same results with that done with the nodal discontinuous Galerkin time-domain (DGTD) method

When making the transition to the Slip Ring Resonator, the resonant absorption cross section drops only slightly, whereas the resonant scattering cross section decreases substantially.The resonant extinction cross section is much lower for the Slip Ring Resonator than for the straight dipole antenna.

Considering the distribution of the charge oscillating with the frequency of the incident wave, the electric-dipole moment of the nano-structure is proportional to the distance between negative and positive charges at the two ends. Evidently, the dipole moment of the straight dipole antenna is bigger than that of the split-ring resonator. Consequently, scattering cross section of the straight dipole antenna, which changes like the square of the dipole moment, should be bigger than that of the split-ring

resonators.

Accordingly, it is believed that the dipole antenna has the larger radiation resistance than the split-ring resonator. In comparison, because the structure total lengths are almost the same, the Ohmic resistances of dipole antenna and split-ring resonators are close to each other, which is equivalent to comparable resonant absorption cross sections.

3.4 Similarity between Apertures and Nanoparticles

3.4.1 Introduction

In this part, the response of apertures and nanoparticles with the identical dimensions is compared and we will prove that apertures and nanoparticles behave in a similar fashion. And the extinction, absorption and scattering for both of apertures and nanoparticles are under single channel limit.

3.4.2 Simulation Details

The cross section of the aperture and nanoparticles were compared when the dimensions are 200nm(length) ,10nm(width) and 50nm(thickness).

For the 200nm By 10nm By 35nm nanoparticle(Material: Au(Palic 0-2um)),

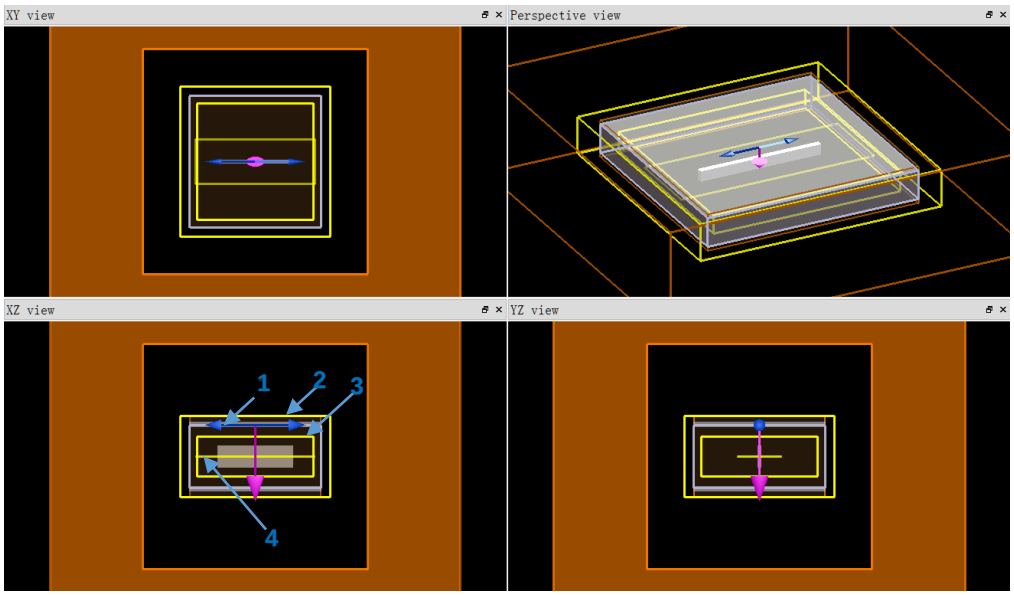

Fig 3.19: TFSF source perpendicular to the short edge of the metal nanoparticles 2: monitor recording the total scattering. 3: monitor recording the total absorption 4: monitor recording the E field.

The cross section is as follows

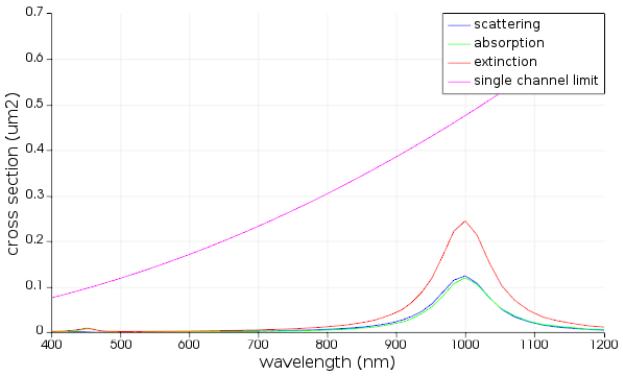

Fig 3.20 The crests of curve for the absorption, scattering and extinction are at 1000nm.The cross section of the absorption and scattering is around $0.12\mu m^2$ and that of extinction is around $0.24\mu m^2$, all of which are under the single channel limit ($0.48\mu m^2$ at 1000nm)

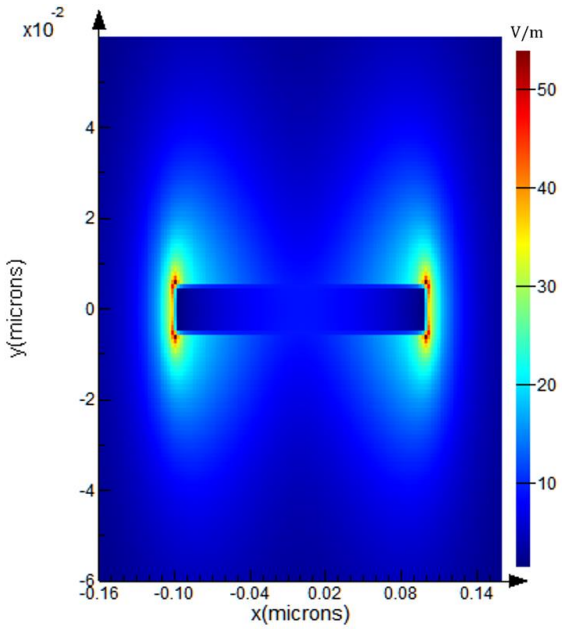

Fig 3.21 we can see that the E field profile for the metal particles in the above picture. The maximum E field happens at the two ends of the rod, and the maximum value is at 54 V/m.

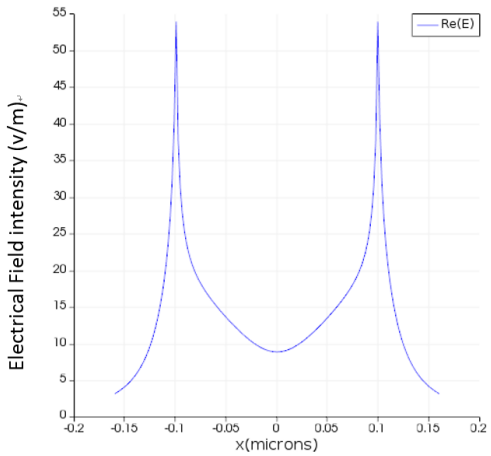

Fig 3.22 the maximum E field happens at the two ends of the rod, and the maximum value is at 54 V/m.

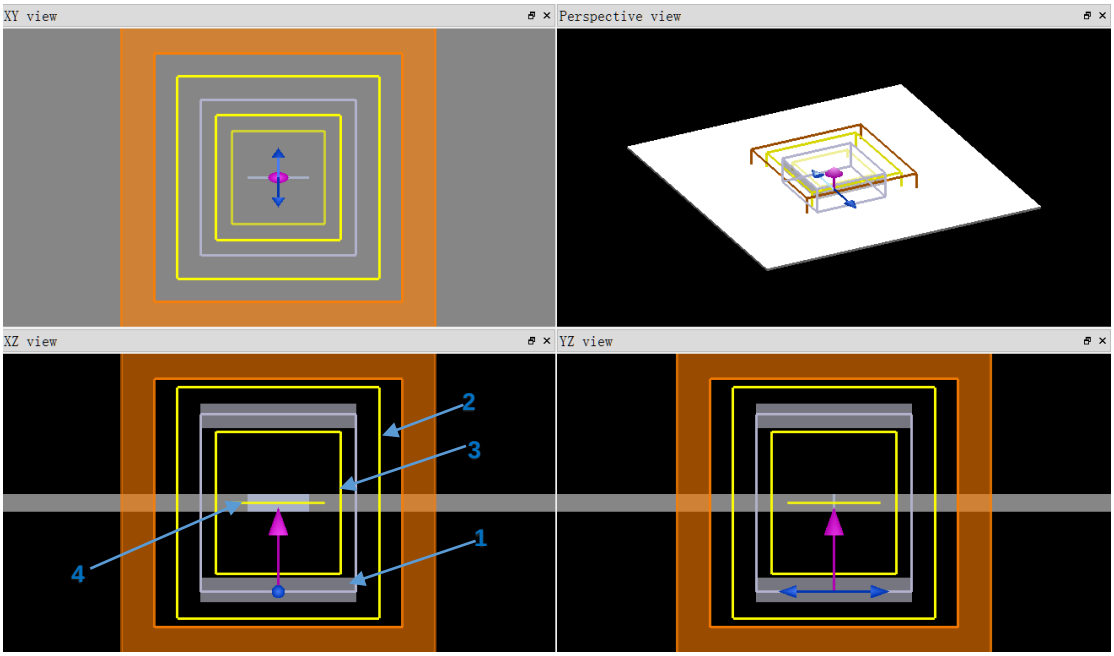

Fig 3.23 the 200nm by 10nm by 50nm aperture. 1: TFSF source perpendicular to the long edge of the metal nanoparticles. 2: monitor recording the total scattering. 3: monitor recording the total absorption. 4: monitor recording the E field.

The cross section is as follows,

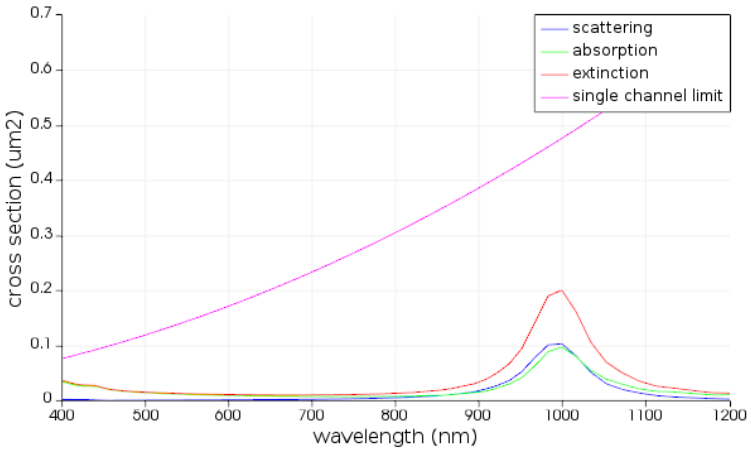

Fig 3.24 the crests of curve for the absorption, scattering and extinction are at 1000nm, which is the same with the crest position in the metal particle case.

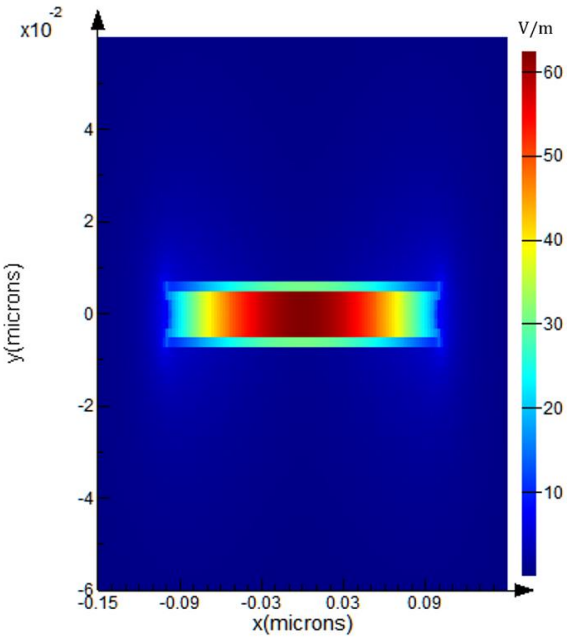

Fig 3.25 the maximum E field happens in the middle of the aperture, and the maximum value is at 62 V/m.

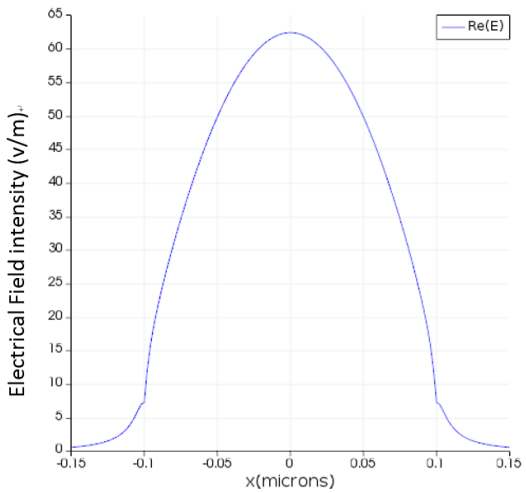

Fig 3.26 the maximum E field happens in the middle of the aperture, and the maximum value is at 62 V/m.

3.4.3 Summary and Discussion

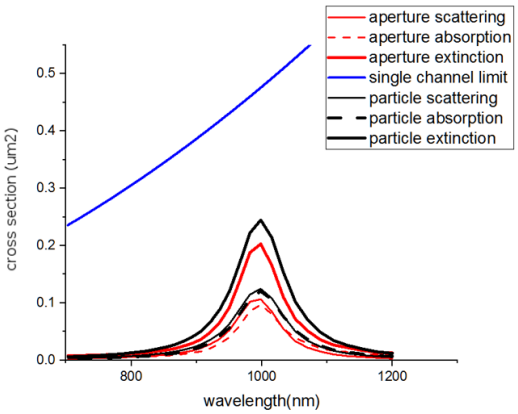

Fig 3.27 The overview of the result

From the figure, the aperture and the nanoparticle share the same position of crest and the same shape of curve. We can say that considering the same dimension ,the aperture and the metal particles behave in a similar fashion. Besides that, the aperture has the stronger maximum E field than the metal particles with the identical dimensions.

3.5 Maximum Absorption of Apertures

3.5.1 Introduction

In this part, we will use FDTD method to prove that the maximum absorption occurs when the absorption equal to the scattering and the absorption cross section is always under single channel limit. For the aperture, the long edge and thickness are fixed at 270nm and 50nm, and I change the width to make the gap between the absorption and scattering different.

3.5.2 Simulation Details

The long edge and thickness are fixed at 270nm and 50nm, and I changed the width

from (20nm to 9nm), the results show below,

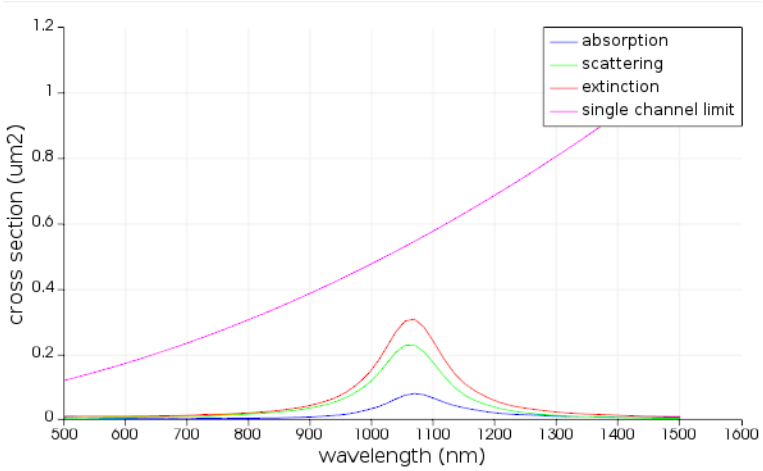

Fig 3.34 At 20nm width ,the absorption cross section is 0.079μm^2.

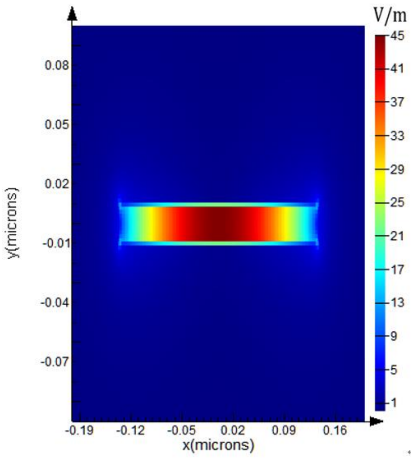

Fig 3.35 The E field in the middle is around 45 V/m.

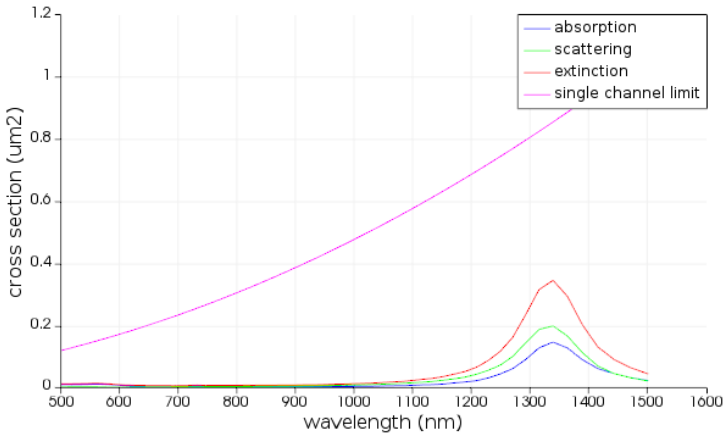

Fig 3.36 At 16nm width, as the absorption went closer to the scattering ,the absorption

cross section is $0.14\mu m^2$

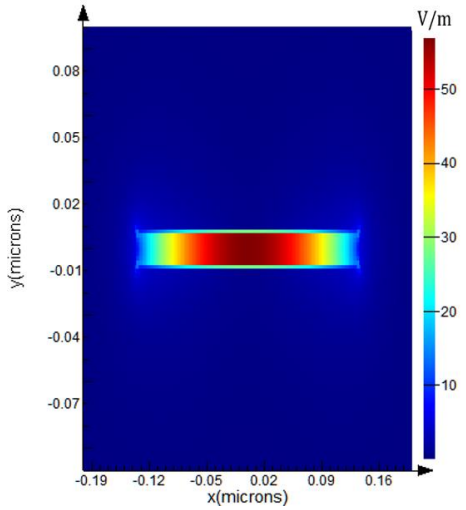

Fig 3.37 The E field in the middle is around 57V/m

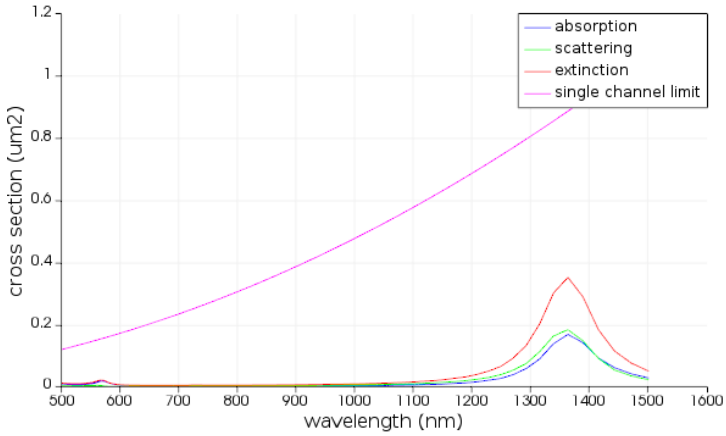

Fig 3.38 At 12nm width, the absorption is almost equal to the scattering, and we see the absorption went to its maximum and the E field in the middle of the structure went to the maximum and the absorption is $0.168\mu m^2$

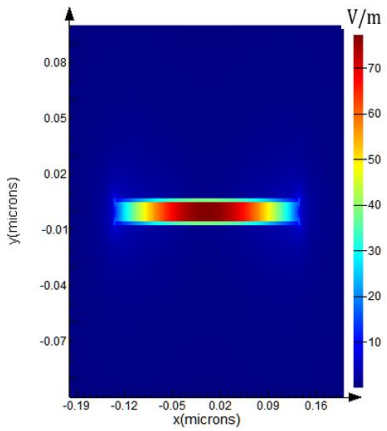

Fig 3.39 The E field is around 77 V/m

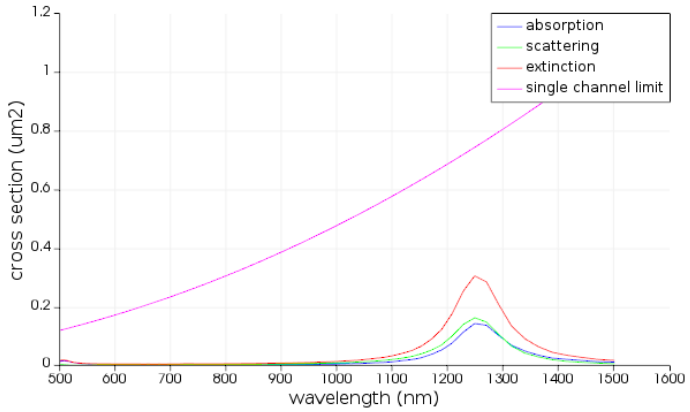

Fig 3.40 At 9nm width, the absorption was getting a little bit further away from the scattering (compared with that at 12nm), and the absorption and the E- field are relatively a little smaller than that of 12nm width .The absorption cross section is 0.142

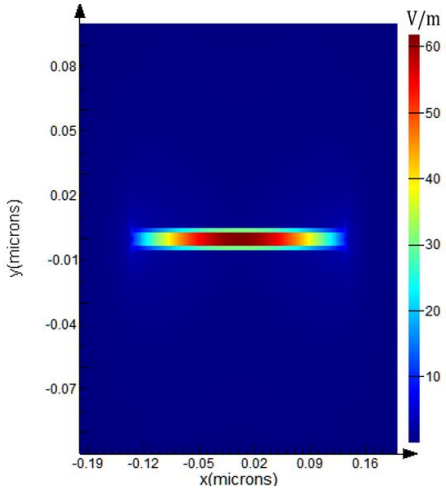

Fig 3.41 The E-field is around 62 V/m

After that, we fixed the width and the thickness as 12nm and 50nm and changed the length (from 300nm to 200nm) in order to make the gap between the scattering and the absorption different.

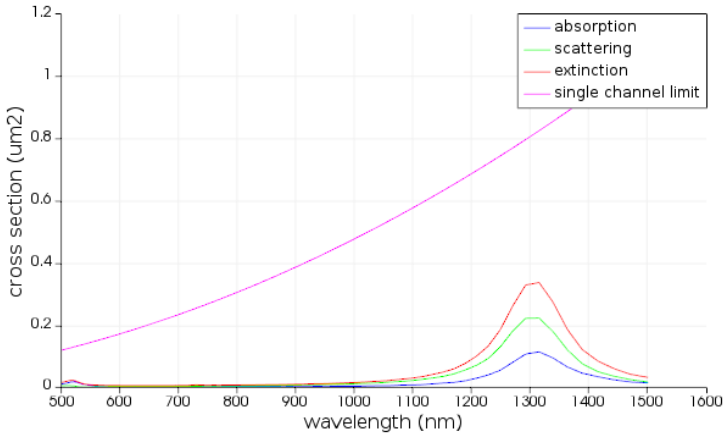

Fig 3.42 At 300nm x 12nm x 50nm, the cross section for the absorption is at 0.1μm^2

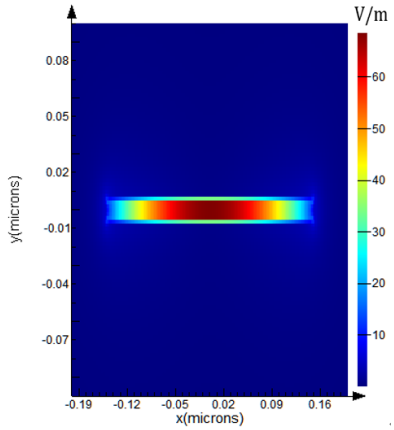

Fig 3.43 The maximum E field is at 68 V/m

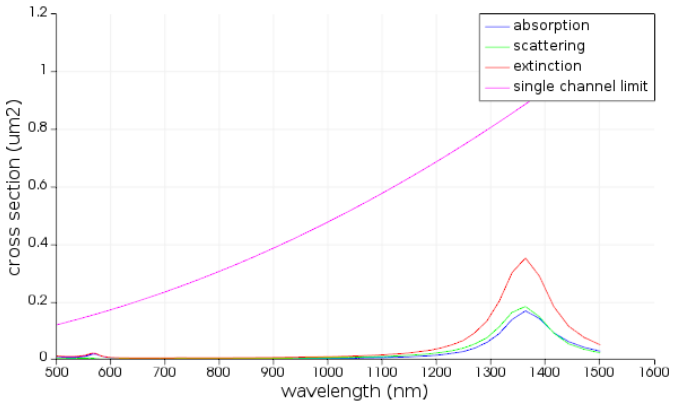

Fig 3.44 At 270nm x 12nm x 50nm (in this case the absorption is almost equal to the scattering), the cross section for the absorption is at 0.18μm^2

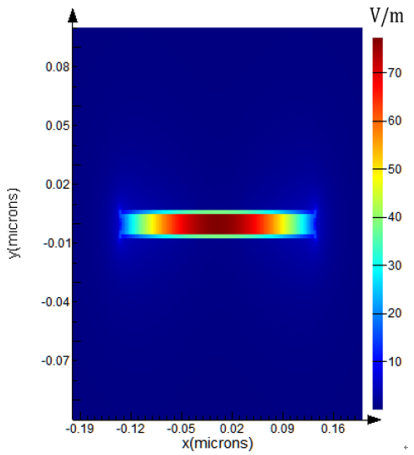

Fig 3.45 The maximum E field is at 77 V/m

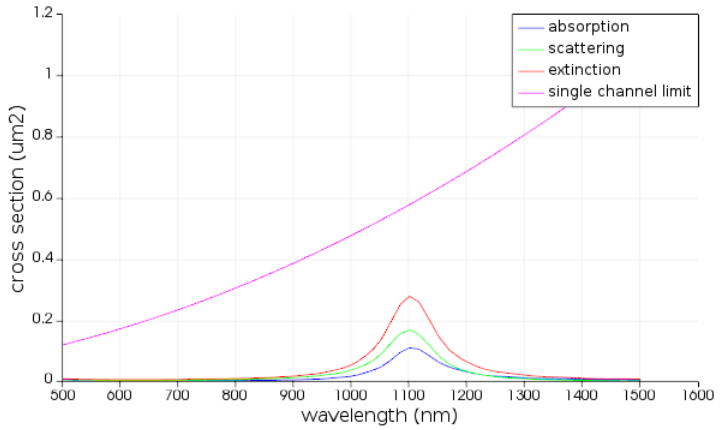

Fig 3.46 At 240nm x 12nm x 50nm, the cross section for the absorption is at 0.1μm^2

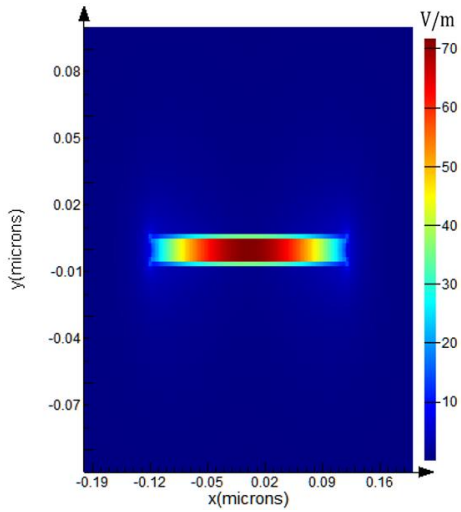

Fig 3.47 The maximum E field is at 72 V/m

3.5.3 Results and Discussion

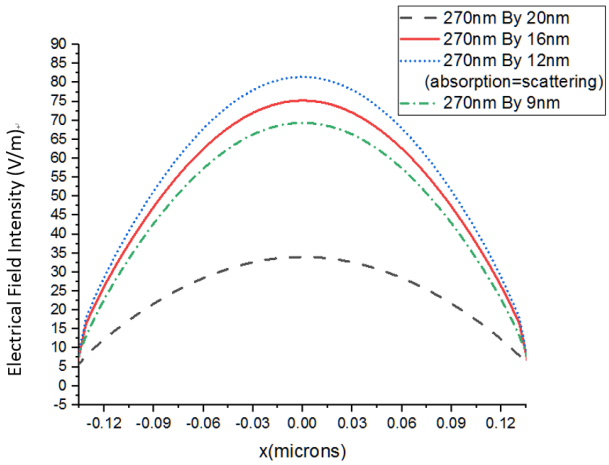

Fig 3.48 The overview of the E fields in the different cases

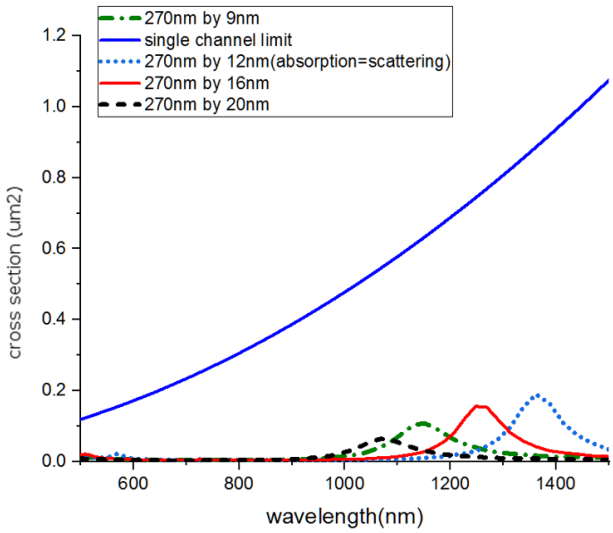

Fig 3.49 The overview of the absorption cross section in the different cases

we can clearly see that the absorption goes to its maximum and the E field in the middle of the structure goes to the maximum when the absorption equals to the scattering.

Chapter 4 Derivation of the theory

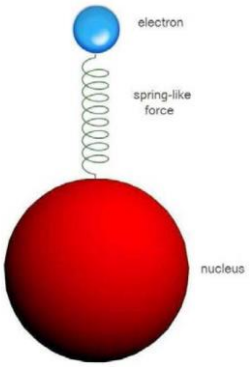

Fig 4.1 Lorentz Oscillator Model for Scattering “Size”

m:electron mass K:restoring force

x:electron displacement e:electron charge

y:damping

$$m\ddot{x} + m\gamma\dot{x} + kx = -eE_0e^{-i\omega t} \tag{4.1}$$

$$\mathrm{x} = x_0e^{-i\omega t} \tag{4.2}$$

$$(-\mathrm{m}\omega^2 - i\omega m\gamma + k)x_0e^{-i\omega t} = -eE_0e^{-i\omega t} \tag{4.3}$$

$$x_0 = \frac{-eE_0}{m(\omega_r^2-\omega^2-i\omega\gamma)} \tag{4.4}$$

$$\omega_r^2 = \frac{k}{m} \tag{4.5}$$

$$\mathrm{k} = \frac{2\pi}{\lambda} \tag{4.6}$$

$$P_0 = qx_0 = \frac{e^2E_0}{m(\omega_r^2-\omega^2-i\omega\gamma)} \tag{4.7}$$

$$\omega = \omega_r \tag{4.8}$$

$$P_0 = e^2E_0/(-i\omega\gamma m) \tag{4.9}$$

For a 3D Electric Dipole, we have

$$\mathrm{P} = \frac{\mu_0}{4\pi} n |\bar{p}_0|^2 \frac{\omega^4}{3c} \tag{4.10}$$

When no absorption there, $\gamma = \gamma_r$ and power in =power out

$$|-i\omega P_0 \cdot E_0| = \frac{c^2 E_0 k^4 |P_0|^2}{12\pi} \tag{4.11}$$

so we get

$$\gamma_r = \frac{e^2 E_0 K_0^2}{6\pi m} \tag{4.12}$$

$\vec{P} = \alpha \vec{E}$ α:polarizability

$$\alpha = \frac{\vec{P}}{\vec{E}} = \frac{6\pi}{E_0 k^2 \omega_r} \tag{4.13}$$

$$\sigma_s = \frac{k^4}{6\pi} \left| \frac{\alpha}{\varepsilon_0} \right|^2 = \frac{3\lambda^2}{2\pi} \tag{4.14}$$

$$I^2 R = P_{abs} \tag{4.15}$$

$$P_{abs} \propto X_0^2 \gamma_a \quad X_0^2 \propto I^2 \quad \gamma_a \propto R$$

$$x_0 = \frac{-eE_0}{m(-i\omega_r \gamma)} \ (\text{at } \omega = \omega_r) \tag{4.16}$$

$$\gamma = \gamma_r + \gamma_a \tag{4.17}$$

when $\frac{\partial P_{abs}}{\partial \gamma_a} = 0$, we get the maximum absorpiton there,

so we have

$$\frac{\partial P_{abs}}{\partial \gamma_a} = \frac{\partial}{\partial \gamma_a}(X_0^2 \gamma_a) = \frac{\partial}{\partial \gamma_a}\left(\frac{\gamma_a}{\gamma^2}\right) = \frac{\partial}{\partial \gamma_a}\left(\frac{\gamma_a}{(\gamma_a+\gamma_r)^2}\right) = \frac{1}{(\gamma_a+\gamma_r)^2} - \frac{2*\gamma_a}{(\gamma_a+\gamma_r)^2} = 0 \tag{4.18}$$

$$\gamma_a = \gamma_r \tag{4.19}$$

Quasi-static derivation

Spatial derivatives dominate:

$$\nabla \times \vec{E} \cong 0, \vec{E} = -\nabla V \tag{4.20}$$

Solution satisfying boundary conditions:

$$V=-E_1 r\cos\theta \qquad r< a \tag{4.21}$$

$$V=E_0 r\cos\theta + \frac{A}{r^2}\cos\theta \quad r> a \tag{4.22}$$

where $E_1 = \frac{3\varepsilon_2 E_0}{\varepsilon_1+2\varepsilon_2}$

V outside contains the potential of a dipole and the polarizability of the dipole is given by:

$$\alpha = 4\pi\epsilon_0 \frac{\epsilon_1-\epsilon_2}{\epsilon_1+2\epsilon_2} a^3 \tag{4.23}$$

this polarizability gives infinite scattering if $\epsilon_1 + 2\epsilon_2 = 0$ (4.24)

(surface plasmon resonance)

including retardation(Mie) to low order gives:

$$\alpha = \frac{4\pi\epsilon_0 a^3(\epsilon_1-\epsilon_2)(1-0.1q^2)}{(\epsilon_1+2\epsilon_2)-(0.7\epsilon_1-\epsilon_2)q^2-(\epsilon_1-\epsilon_2)i2q^3/3} \tag{4.25}$$

where q=ka

$$\alpha_{max} = \frac{i6\pi\epsilon_0}{k^3} \tag{4.26}$$

The maximum scattering cross section is then:

$$C_{scat,max} = \frac{k^4\left|\frac{\alpha_{max}}{\epsilon_0}\right|^2}{6\pi} = \frac{3\lambda^2}{2\pi} \tag{4.27}$$

same result for resonance fluorescence

Chapter 5 Conclusion

1. With the 100nm silver film we can see the redshift in the transmission peak wavelength by cutting down width of the hole and we can also observe that transmittance is increasing with the ratio the length of the long edge over the length of the short edge.

2. For the aperture ,the forward scattering is equal to the backward scattering, and both of them are under the single channel limit

3. With the FDTD method, it is proved again that when we changed the shape of the particle, the relation between the absorption and the scattering changed. As changing the shape of the structure (from straight nanostructure to Split Ring Resonance), the scattering is increasing while the absorption is decreasing and eventually the absorption exceeds the scattering. For each case, the extinction, the scattering and the absorption are all under the single channel limit. With the FDTD method, we can see the same results with that done with the nodal discontinuous Galerkin time-domain (DGTD) method.

4. Apertures and nanoparticles behave in a similar fashion, and the aperture has the stronger maximum E field compared to the metal particles with the identical dimensions.

5 Maximum absorption occurs when the absorption is equal to the scattering, and the E field in the middle of the structure reaches the maximum at the same time. In all of our simulation case, we used a single aperture system, whose extinction, scattering and absorption were limited by the single channel limit.

The single channel limit and beyond[26]

It is known that the single channel limit for 2D transmission is λ/π ,and there is also a reflected component with equal contribution.

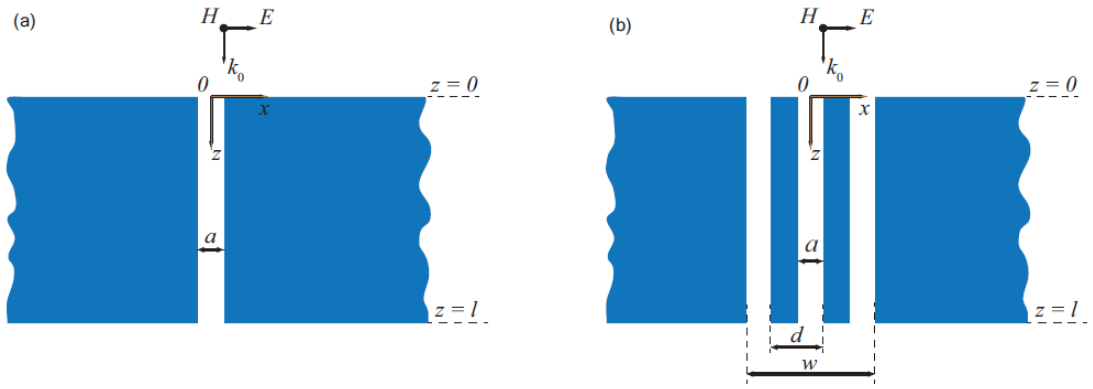

Fig 5.1 An instance of subwavelength multi-slit system was shown. Three subwavelength slits were included ,which were separated by d in an infinitely wide metallic film with the thickness l. The dimensions are normalized to the incident wavelength.

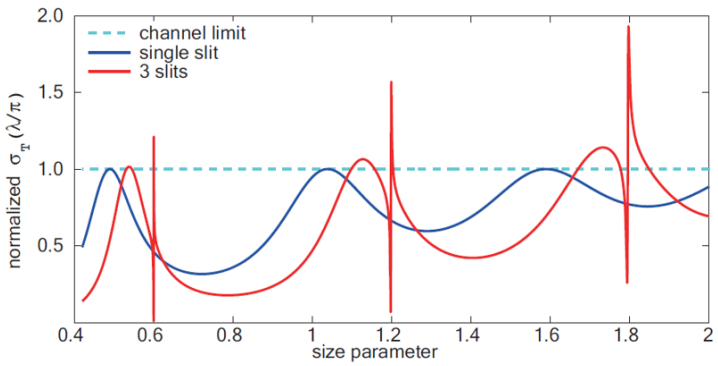

Fig 5.2 The contrast of transmissions with the single channel limit was shown. The dimension of the two slit systems is 1 um in length and 0.2 um in width. The size parameter means to the ratio of the total width and wavelength. The cross sections of

the transmission are normalized to λ/π.

It was also shown that super-transmission in a three slit system exceeded the single channel limit. Two transmission resonances existed at the same time in the three slit system with symmetric or asymmetric distribution. On one hand, the transmission with symmetric features is basically confined by the single channel limit. On the other hand, the transmission with asymmetric features shows larger cross section than the single channel limit. Fano resonance can explain the origin of the asymmetric resonance[27]. Two different scattering channels coupling through the diffraction at the ends of the slits were supported by the three slits. As we all know, π phase jump exists around the resonance, which shows in-phase and out-phase interference producing enhanced and reduced transmission individually.

Another result can be shown in Fig 5.1 that the total width of the three slit system is the same with the that of single slit. More light was transmitted by the three slits transmits than by the single slit.

Reference

[1] Yee, Kane. "Numerical solution of initial boundary value problems involving Maxwell's equations in isotropic media." *IEEE Transactions on antennas and propagation* 14.3 (1966): 302-307.

[2] Taflove, Allen, and Morris E. Brodwin. "Numerical solution of steady-state electromagnetic scattering problems using the time-dependent Maxwell's equations." *IEEE transactions on microwave theory and techniques* 23.8 (1975): 623-630.

[3] Taflove, Allen, and Morris E. Brodwin. "Computation of the electromagnetic fields and induced temperatures within a model of the microwave-irradiated human eye." *IEEE Transactions on Microwave Theory and Techniques* 23.11 (1975): 888-896.

[4] Holland, Richard. "THREDE: A free-field EMP coupling and scattering code." *IEEE Transactions on Nuclear Science* 24.6 (1977): 2416-2421.

[5] Mur, Gerrit. "Absorbing boundary conditions for the finite-difference approximation of the time-domain electromagnetic-field equations." *IEEE transactions on Electromagnetic Compatibility* 4 (1981): 377-382.

[6] Higdon, Robert L. "Absorbing boundary conditions for difference approximations to the multidimensional wave equation." *Mathematics of computation* 47.176 (1986): 437-459.

[7] Betz, Vaughn, and Raj Mittra. "Comparison and evaluation of boundary conditions for the absorption of guided waves in an FDTD simulation." *IEEE Microwave and Guided wave letters* 2.12 (1992): 499-501.

[8] Berenger, Jean-Pierre. "A perfectly matched layer for the absorption of electromagnetic waves." *Journal of computational physics* 114.2 (1994): 185-200.

[9] Teixeira, Fernando L. "Time-domain finite-difference and finite-element methods for Maxwell equations in complex media." *IEEE Transactions on Antennas and Propagation* 56.8 (2008): 2150-2166.

[10] Holland, Richard, and Larry Simpson. "Finite-difference analysis of EMP coupling to thin struts and wires." *IEEE Transactions on electromagnetic compatibility* 2 (1981): 88-97.

[11] Simpson, Jamesina J., and Allen Taflove. "Electrokinetic effect of the Loma Prieta earthquake calculated by an entire-Earth FDTD solution of Maxwell's equations." *Geophysical*

research letters 32.9 (2005).

[12] Gedney, Stephen D. "Introduction to the finite-difference time-domain (FDTD) method for electromagnetics." *Synthesis Lectures on Computational Electromagnetics* 6.1 (2011): 1-250.

[13] Sarkar, Tapan K., and Odilon Pereira. "Using the matrix pencil method to estimate the parameters of a sum of complex exponentials." *IEEE Antennas and Propagation Magazine* 37.1 (1995): 48-55.

[14] Cockburn, Bernardo, George E. Karniadakis, and Chi-Wang Shu. "The development of discontinuous Galerkin methods." *Discontinuous Galerkin Methods*. Springer, Berlin, Heidelberg, 2000. 3-50.

[15] Hesthaven, Jan S., and Tim Warburton. "High-order nodal discontinuous Galerkin methods for the Maxwell eigenvalue problem." *Philosophical Transactions of the Royal Society of London A: Mathematical, Physical and Engineering Sciences* 362.1816 (2004): 493-524.

[16] Ruan, Zhichao, and Shanhui Fan. "Superscattering of light from subwavelength nanostructures." *Physical review letters* 105.1 (2010): 013901

[17] C. J. Foot, 2005 .*Atomic Physics* . Oxford University Press ,New York, pp. 140–142.

[18] F. J. García-Vidal, L. Martín-Moreno, Esteban Moreno, L. K. S. Kumar, and R. Gordon. "Transmission of light through a single rectangular hole in a real metal." *Physical Review B* 74.15 (2006): 153411.

[19] F. J. García-Vidal, Esteban Moreno, J. A. Porto, and L. Martín-Moreno. "Transmission of light through a single rectangular hole." *Physical review letters* 95.10 (2005): 103901.

[20]Gordon, R., L. Kiran Swaroop Kumar, and Alexandre G. Brolo. "Resonant light transmission through a nanohole in a metal film." *IEEE Transactions on Nanotechnology* 5.3 (2006): 291-294.

[21] Koerkamp, KJ Klein. "KJ Klein Koerkamp, S. Enoch, FB Segerink, NF van Hulst, and L. Kuipers, Phys. Rev. Lett. 92, 183901 (2004)." *Phys. Rev. Lett.* 92 (2004): 183901.

[22] Cao, Hua, and Ajay Nahata. "Influence of aperture shape on the transmission properties of a periodic array of subwavelength apertures." *Optics express* 12.16 (2004): 3664-3672.

[23] A.Degirona, H.J.Lezeca, N.Yamamotob, T.W.Ebbesen. "Optical transmission properties of

a single subwavelength aperture in a real metal." *Optics Communications* 239.1-3 (2004): 61-66.

[24] Martin Husnik, Stefan Linden, Richard Diehl, Jens Niegemann, Kurt Busch, and Martin Wegener "Quantitative experimental determination of scattering and absorption cross-section spectra of individual optical metallic nanoantennas." *Physical review letters* 109.23 (2012): 233902.

[25] M. G. Nielsen, A. Pors, R. B. Nielsen, A. Boltasseva, O.Albrektsen, and S. I. Bozhevolnyi, Opt. Express 18, 14 802 (2010).

[26] Chen, Shuwen, Shilong Jin, and Reuven Gordon. "Super-transmission from a finite subwavelength arrangement of slits in a metal film." *Optics Express* 22.11 (2014): 13418-13426.

[27] Yong Xie, Armis R. Zakharian, Jerome V. Moloney, and Masud Mansuripur. "Transmission of light through slit apertures in metallic films." *Optics Express* 12.25 (2004): 6106-6121.